

Atmospheric Measurements aboard C-130 During the Pacific Atmospheric Sulfur Experiment

Anastasia G. Yanchilina

Department of Atmospheric Science, Creighton University, Fall 2007

SOARS[®] Summer 2007

Science Research Mentor: Lee Mauldin

Writing and Communication Mentors: Paul Kucera and Rob Markel

Community Mentor: Reta Lorenz

Peer Mentor: Armand Silva

ABSTRACT

The Pacific Atmospheric Sulfur Experiment (PASE) is a study with a primary goal aimed at understanding the sulfur cycle in a remote marine atmosphere. The study will be conducted in August and September months of 2007 at Christmas Island on board the NSF/NCAR C-130 aircraft. It will foremost focus on measurements of DMS (dimethyl sulfide) and its contribution to formation of H₂SO₄ (sulfuric acid) and MSA (methane-sulfonic acid) by reaction with OH (hydroxyl). PASE will also concentrate on subsequent production of aerosols and cloud condensation nuclei from H₂SO₄, MSA, and NH₃ concentrations in a cloud free convective boundary layer (CBL) and in outflow of marine cumulus. This paper explains the measurement technique for OH, H₂SO₄, MSA, HO₂, HO₂+RO₂ (peroxy radicals), and NH₃ (ammonia) using the SICIMS (Selected ion chemical ionization mass spectrometer). It also presents sample measurements from test flights of OH, H₂SO₄, MSA, HO₂, and HO₂+RO₂. In addition, this paper discusses the measurement technique utilized aboard the C-130 in testing SO₂, DMS, DMSO (dimethyl sulfoxide), DMSO₂ (dimethyl sulfone), O₃ (ozone), aerosols, and cloud condensation nuclei. It includes several adaptations to technique and instrumentation from previous studies conducted: the First Aerosol Characterization Experiment (ACE-1) in 1998, the Pacific Exploratory Missions A and B (PEM-Tropics) in 1996, and the Intercontinental Transport Experiment (INTEX-B) in 2006.

The Significant Opportunities in Atmospheric Research and Science (SOARS) Program is managed by the University Corporation for Atmospheric Research (UCAR) with support from participating universities. SOARS is funded by the National Science Foundation, the National Oceanic and Atmospheric Administration (NOAA) Climate Program Office, the NOAA Oceans and Human Health Initiative, the Center for Multi-Scale Modeling of Atmospheric Processes at Colorado State University, and the Cooperative Institute for Research in Environmental Sciences. SOARS also receives funding from the National Center for Atmospheric Research (NCAR). SOARS is a partner project with Research Experience in Solid Earth Science for Student (RESESS).

1. Introduction

This study describes an improved SICIMS (Selected Ion Chemical Ionization Mass Spectrometer) technique to take airborne measurements of OH, NH₃, H₂SO₄, MSA (CH₃SO₂OH), HO₂, and HO₂+RO₂ on board the NSF/NCAR C-130 as part of the PASE (Pacific Atmospheric Sulfur Experiment) to take place at Christmas Island in summer 2007. The primary goal of PASE is to confirm the CLAW theory [Charlson, Lovelock, Andreae, Warren, 1987] which describes the sulfur cycle in a marine atmosphere, its role in the cloud nucleation processes, and its implications for climate change. In particular, measurements of these chemicals will provide a better understanding of subatomic particle nucleation in the outflow of marine cumulus and photochemical processes in a remote boundary layer of the atmosphere.

The implications for climate change arise from the formation of aerosols and cloud condensation nuclei from the oxidation products of DMS (dimethyl sulfide) and ammonia through the direct and indirect processes. The direct method includes the aerosols' role in mainly reflecting and scattering the incoming solar radiation while the indirect method (also known as the Aerosol Indirect Effect) includes the role of cloud condensation nuclei in formation of clouds and subsequent albedo increase. Thus, measurements from PASE will try to provide a connection between the sulfur chemistry and the evolution of aerosols.

The chemical composition of the atmosphere is largely dependent upon the capacity of OH to oxidize many gases to products more easily removed by precipitation and dry deposition at the earth's surface [Lelieveld, 2004]. The hydroxyl radical forms as a result of its interaction with H₂O and O₂ which occurs from photolysis of O₃ in the 290-340 nm spectral region (R1, R2).



Measurement of OH also allows for simultaneous measurement of MSA and H₂SO₄. In application to the PASE campaign, OH is the primary radical which causes the oxidation of DMS to MSA and SO₂ during daytime. OH oxidizes DMS to SO₂ and MSA and H₂O₂, HO₂NO₂, and OH oxidize SO₂ to form sulfate (SO₃) which then interacts with water to form H₂SO₄. Measurements of H₂SO₄ and MSA are important as the two can be direct precursors to the formation of atmospheric submicrometer sulfate particles which act to reduce solar radiation by backscattering or by increasing cloud albedo [Schwartz, 1996; Kulmala et al., 2000].

Understanding the cycling of NH₃ is significant in order to understand its effects on acid deposition, enhanced aqueous SO₂ oxidation, aerosol and cloud condensation nuclei formation, production of nitrous oxide in remote atmosphere, and redistribution of nutrient nitrogen in biospheric systems [Krupa, 2003]. The cycling of gas phase ammonia in the atmosphere is controlled through its equilibrium with aerosol species such as NH₄NO₃ and (NH₄)₂SO₄ and with aqueous droplets via NH₃(g) ↔ NH₃(aq) ↔ (⁺NO₃⁻)(aq) + (NH₄⁺) ↔ NH₄NO₃² [Schendel, 1990].

¹D refers to an excited Oxygen atom—the singlet oxygen atom. ¹Δ and ³Σ refer to metastable molecular stages.
² (g) refers to a gas state and (aq) refers to an aqueous state

HO₂ + RO₂—also known as peroxy radicals—result through the oxidation of hydrocarbons in the atmosphere as shown in reactions R3, R4, R5, R6. M in these reactions stands for any third body that carries away energy whereas R stands for an organic carbon fragment. Measurements of these concentrations can help explain the transfer of peroxy radicals and their interaction with other gases in the atmosphere.



Peroxy radicals also govern the production and loss of O₃ in the atmosphere [Edwards *et al.*, 2003]. Through interaction with NO, RO₂ and HO₂ produce RO, OH, and NO₂ as shown in R7-R11. The photolysis of NO₂ in turn produces oxygen. Thus, measurements of peroxy radicals directly correspond to understanding part of the ozone and NO_x cycling in the troposphere.



Due to their low concentrations, high reactivity and short lifetimes, direct measurements of OH, NH₃, and HO₂ and RO₂ have only been possible over the last couple decades. During this study, OH concentrations were determined by the use of SICIMS (Selected Ion Chemical Ionization Mass Spectrometer) [Mauldin *et al.*, 1998; Tanner *et al.*, 1997], and HO₂ and RO₂ using a PerCIMS (Peroxy Radical Chemical Ionization Mass Spectrometer) [Edwards *et al.*, 2003]. Previous estimates of the uncertainties of these measurements include ±40% accuracy (2 sigma) for all species mentioned above.

This study will extend the knowledge gained from previous airborne campaigns conducted with the participation of an SICIMS instruments which include the First Aerosol Characterization Experiment) in 1998, PEM-Tropics A and B (Pacific Exploratory Mission) in 1996, and INTEX-B (Intercontinental Transport Experiment) in 2006.

2. Methodology

Techniques utilized for the measurement of SO₂, DMS, DMSO, DMSO₂, OH, H₂SO₄, MSA, NH₃, HO₂, HO₂+RO₂, O₃, aerosols, and cloud condensation nuclei will be described. Also will be mentioned some difficulties associated with measurements of these species and the inlets used in transporting them for detection and analysis.

a. Measurement of DMS, DMSO, DMSO₂, SO₂

³ ³P refers to the ground electronic states of oxygen

1) INLETS

DMS, DMSO, DMSO₂, SO₂ are measured using three separate APIMS (Atmospheric Pressure Chemical Ionization Mass Spectrometer) instruments. All three systems utilize a rearward facing Teflon inlet located on the forward section of the C-130. The inlets face backwards to exclude the entrance of water droplets and particulates. The inlets are also heated to minimize interferences caused by these compounds sticking to the inlet wall and then re-evaporating at a later time.

2) TECHNIQUE

The APIMS instrument is based on a differentially pumped quadrupole mass spectrometer composed of four different pressure zones [Thornton *et al.*, 2002]. The schematic for the instrument is shown in Figure 1. The ionization takes place at ambient pressure. The three pumping regions are the: 1. the declustering section between the ionization region and the mass spectrometer which is pumped by a rotary pump, 2. the ion drift region which is pumped by turbo pumps, 3. the region containing the quadrupole and the detector which is pumped by a turbo pump.

All of the three measurements utilize three slightly different ionization techniques. For the measurement of SO₂, a certain amount of ozone is let in upstream of the ionization region. The ozone level achieved is high enough so that the sensitivity does not change the amount of ozone in ambient air [Thornton *et al.*, 2002]. The ozone is ionized to O₂⁻ by passing through a ⁶³Ni source. It will interact with CO₂ to form CO₃⁻. Consequently, CO₃⁻ will react with SO₃⁻ forming SO₅⁻, an ion which will be quantified by mass spectrometer after leaving the ionization and declustering region. One of the challenges in making the measurements is the higher concentration of water vapor in the marine boundary layer [Thornton *et al.*, 2002]. This is overcome by drying the sample. Furthermore, a known concentration of ³⁴SO₂ is added which allows for continuous monitoring of the instrument sensitivity and facilitated high transmission of SO₂ [Thornton *et al.*, 2002].

DMS and DMSO are determined using very similar techniques as are those utilized in determining SO₂. Instead of generating a negative ion as is the case in the detection of SO₂, this technique generates a positive ion—hydronium—by protonation of water [Bandy *et al.*, 2002]. This technique also utilizes ⁶³Ni as the ion source. Ionizing radiation at atmospheric pressure produces protonated water clusters. Specifically, water clusters at mass 55 (3 water molecules) and 73 (4 water molecules) predominate. DMS is protonated by the mass 55 water cluster to produce DMSH⁺ (mass 63). DMSO becomes DMSOH⁺ (mass 79). The ions DMSO and DMSOH are the quantified by mass spectrometry.

As H₂O levels increase and higher hydrates form, the stability of the hydrates of DMSH⁺ decreases rapidly relative to stability of H₃O⁺ [Bandy *et al.*, 2002]. Increasing H₂O shifts the equilibrium of equation to the left leading to decreased sensitivity at high H₂O levels [Bandy *et al.*, 2002]. Similarly to the technique in sampling SO₂, the air is dried to a dew point below -30°C [Bandy *et al.*, 2002].

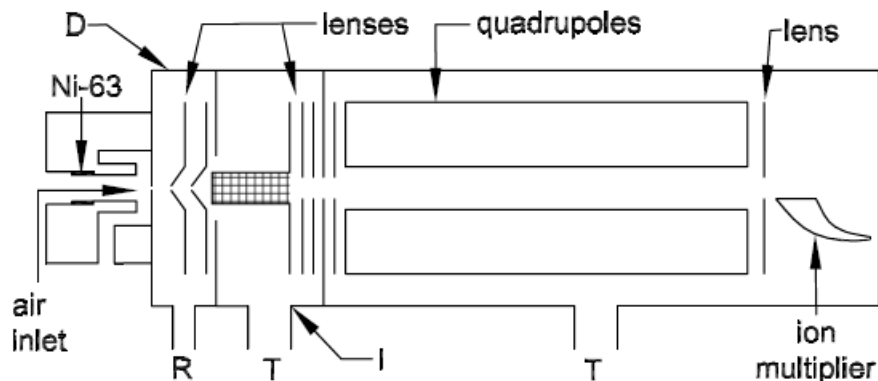


Figure 1: This depicts the basic construction of the APIMS used in sampling SO_2 , DMS, DMSO, and DMSO_2 . D is the declustering region, R is the rotary pump, I is the ion drift region pumped by turbo pumps T. [Thornton *et al.*, 2002].

b. Measurement of OH, H_2SO_4 , MSA, NH_3 , HO_2 , HO_2+RO_2

1) INLETS

The sampling ducts for the three inlet channels share the same function but are different in their structures because of the different chemical properties of gases measured.

The OH, H_2SO_4 , and MSA sampling has to be positioned nearly parallel to the flow because transportation of OH and H_2SO_4 has to be relatively quick as these gases have very short lifetimes in the atmosphere. At the same time, the sampling duct minimizes flow separation, straightens the flow and makes it nonturbulent which is necessary to keep OH and H_2SO_4 from reacting with other molecules and with the walls of the sampling duct. This is accomplished via the use of two cylindrical inner ducts and elliptical surfaces. The inlet is tilted at an angle of 9-10°. By bending the sample airflow, the water droplets would hit the walls of the inlet because they would follow straight trajectories. This inlet also functions at ambient pressure. A more thorough description of the inlet can be found in [Eisele *et al.*, 1997]. The air flow is pumped down by the virtual iris, positioned at the end of the drift tube before its entrance into the collisional dissociation chamber, which will be discussed later.

The construction of the NH_3 sampling duct is similar to the OH inlet. It also contains two cylindrical ducts located to the rear of the flow necessary for flow reduction. The main difficulty encountered with this measurement is that NH_3 is an extremely sticky molecule as a result of its polar nature and thus often sticks to the walls of the sampling duct. Thus, high speed needs to be maintained. One major difference is that this sampling duct possesses only one set of elliptical surfaces to straighten the flow and minimize its separation. This is because the air flow has to be turbulent in order to make the concentration of NH_3 molecules more evenly distributed. The chemical ionization region of the NH_3 to NH_4^+ and the pinhole pump that follows it are located to the rear of the sampling duct. The pinhole pump which sucks in the air flow with the ions formed.

The HO₂, HO₂+RO₂ inlet is placed orthogonal to the flow and thus reduction of the speed of the air flow is not necessary. Such direction of the inlet is possible because the peroxy radicals have slightly longer lifetimes and are not as reactive as the OH radical. One main difference is that while the chemical reaction and ionization regions of the NH₃ and OH inlets take place at ambient pressure, this inlet functions at a reduced pressure of 150 Torr (mm Hg). A reduction of pressure in the inlet is necessary because such a condition is more favorable for chemical reaction and ionization to take place.

2) TECHNIQUE

The technique used for measurement of these chemical species is chemical ionization which is different for each. NH₃ is ionized via the utilization of two corona needles. The corona needles create a plasma around them which ionize NH₃ to NH₄⁺ ions. The ions then enter the CDC, and get transported to the mass spectrometer via an octopole. The mass spectrometer will select specific ions via an application of radio frequency and direct current voltage. The channeltron is used for the detection of the ions. OH, H₂SO₄, and MSA are measured via addition of HNO₃ to sample airflow. The measurement of OH includes the addition of ³⁴SO₂ in order to distinguish it from the naturally occurring SO₂. HNO₃ will pass through a region of ²⁴¹Am which ionizes it to NO₃⁻. This ion will interact with H₂³⁴SO₄, H₂SO₄, and MSA in formation of H³⁴SO₄⁻, HSO₄⁻, and MSA⁻, respectively. These will then be analyzed and detected via the same technique as described for ammonia. For the HO₂ and the HO₂+RO₂ measurements, added concentrations of O₂, SO₂, and NO will determine the sensitivity to RO₂ which will allow for differentiation between HO₂ and HO₂+RO₂ modes. The reactions with NO and SO₂ will convert the HO₂ or the HO₂+RO₂ radicals to H₂SO₄. An amount of HNO₃ will then be added and ionized by ²⁴¹Am to NO₃⁻. The nitrate ion will then react with H₂SO₄ in formation of HSO₄⁻ which will be quantified by mass spectrometry. A more specific description of the inlets and the chemical ionization technique for the SICIMS is available in the appendix.

c. Measurement of O₃

1) INLETS

The two inlets for O₃ measurements are located under the belly of the C-130 aircraft away from the exhaust. They are constructed of stainless steel gooseneck snaked with 3/8" tubing used to snug the 1/4" tubing (the inlet itself) into the gooseneck [Pollack, 2007]. The gooseneck is curved so that the tip points either fore or aft and is located 10" from the surface of the belly of the aircraft which allows the sampling of air from outside the boundary layer of the aircraft.

One of the inlets faces rearward and is used for the slow response O₃ instrument. Such position inhibits the entrainment of large particles into the instrument [Pollack, 2007]. The air is pulled in through the use of a pump which permits adequate flow through the spectrometer. The other inlet faces forward and acts as a bypass line for the fast response of the O₃ instrument, picking up ambient air. The bypass line consists of a 640 Torr control valve and two small diaphragm pumps [Pollack, 2007]. The two pumps pump down the pressure in the inlet while

the control valve controls the pressure at that particular level. This allows the flow through it to be approximately 8 slm (standard liters per minute). The O₃ instrument picks up approximately 0.5 slm from the bypass line [Pollack, 2007]. The bypass line is used to increase the time response of the instrument. Such construction is also utilized for the CO instrument but will not be discussed here.

2) TECHNIQUE

The use of two inlets is used for bringing air into two O₃ instruments, a slow response instrument which employs UV absorption and operates at about 1 Hz and a fast response instrument which employs chemiluminescence and operates at 5 Hz and above.

(i) *Slow response instrument*

The slow response instrument basically consists of a UV lamp, two sample chambers, and the detectors [Profitt and McLaughlin, 1983]. The schematic for the instrument is shown in Figure 2. The lamp emits radiation at 254 nm which is directed to two sample chambers via a beam splitter. Ozone readily absorbs radiation at this wavelength. Changes in ozone concentration in either of the chambers will produce a change in intensity at its detector [Profitt and, McLaughlin, 1983]. Its $1.5 \times 10^{10} \text{ cm}^{-3}$ precision translates into a precision of ± 2.3 ppbv with an overall uncertainty of 3% [Pollack, 2007]. UV optical components, contained within the pressurized lamp, split and align the beam along the center of each flow cell by a combination of beam splitter and a mirror [Pollack, 2007]. The flow system has wetted Teflon parts which will reduce ozone wall losses to minimal levels [Pollack, 2007]. A catalytic ozone scrubber is used to quantitatively remove ozone from air directed through the blank measurement path [Pollack, 2007]. A valve alternates the scrubbed air between the two chambers [Profitt and, McLaughlin, 1983]. The flow exits the two chambers through to an exhaust, pumped out by gear pumps.

By using an ozone scrubber, an ozone-free air sample is directed into one chamber, while unaltered air is directed into another [Profitt and, McLaughlin, 1983]. A valve alternates the scrubbed airflow between the two chambers. From the measured intensities at the two detectors, the concentration of ozone can then be calculated.

The detector consists of a pair of UV-sensitive photodiodes and their associated circuitry [Profitt, McLaughlin, 1983]. The light striking a photodiode generates a current at the input of the operational amplifier which is proportional to light intensity [Profitt and McLaughlin, 1983].

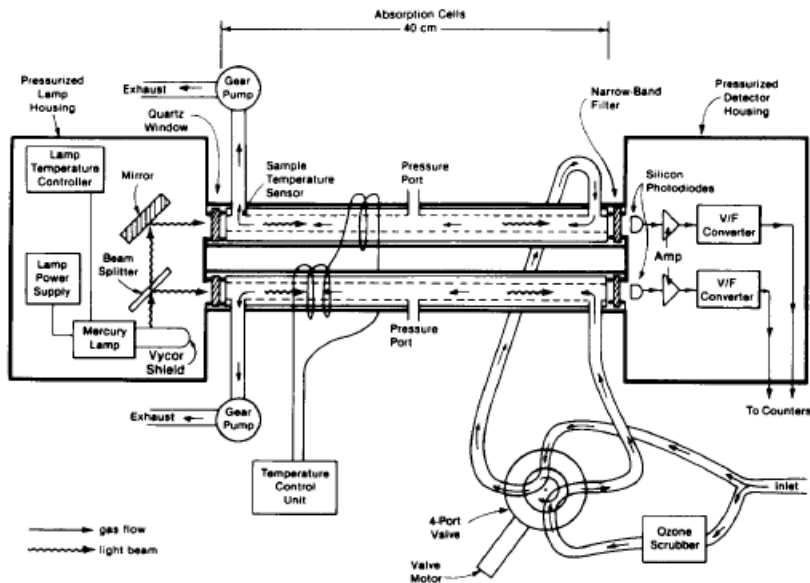


Figure 2: This depicts the design of the instrument [Profitt et al., 1983].

(ii) *Fast response instrument*

The fast response instrument employs chemiluminescence for measuring the O_3 concentrations, which is the detection of the emission of light without the emission of heat as the result of a chemical reaction. The advantage of the chemiluminescence technique relative to the UV absorption is its inherently higher sensitivity and precision [Pollack, 2007].

The heart of the instrument is the reaction vessel which is a conically shaped volume, the end view of which is seen by a dry-ice red-sensitive photomultiplier tube [Ridley et al., 1991]. The schematic for this instrument is depicted in Figure 3. The photomultiplier tube (pmt) is coupled to the reaction vessel through a red cutoff filter. Ambient air enters the reaction vessel through the rear axial inlet. Before entering the conical highly reflective volume, the ambient air is premixed with pure NO reagent gas [Ridley et al., 1991]. The NO reagent gas enters through the inlet orthogonal to the airflow and is supplied from a cylinder kept at a specific pressure [Ridley et al., 1991]. Another port is used to manage the reaction vessel pressure [Ridley et al., 1991]. The gas mixture is pumped from the reaction vessel through a circular annulus which is located at the base of the conical reaction chamber [Ridley et al., 1991].

The equations for the NO- O_3 chemiluminescence signal for detection of NO determine the design of the conical reaction vessel [Ridley et al., 1991]. The activated state of the NO_2 emits light in the wavelengths of visible to infrared as it reverts to a lower energy state [Pollack, 2007]. The chemiluminescent intensity is a function of both pressure and temperature [Ridley et al., 1991]. The pmt is used to detect the signal of O_3 which is proportional to the mixing ratio of O_3 and the sensitivity is proportional to the sample mass of the O_3 detected divided by the reaction vessel pressure [Pollack, 2007]. The pmt is maximized for a specific set of flow conditions, reaction-vessel geometry, and construction [Ridley et al., 1991]. The instrument is operated by a vacuum pump and valve to maintain the reaction vessel.

The sensitivity of instrument is sensitive to water vapor in the reaction vessel [Ridley *et al.*, 1991]. Thus, in warm marine or continental boundary layer atmospheres, the correction of the sensitivity is significant. O₃ data is corrected using the relevant state parameters measured routinely on research aircraft [Ridley *et al.*, 1991]. The standard deviation of the 1-sec measurements, which would include atmospheric variability, is approximately 2 ppbv for the UV instrument and 0.2-0.5 ppbv from the chemiluminescence instrument [Pollack, 2007].

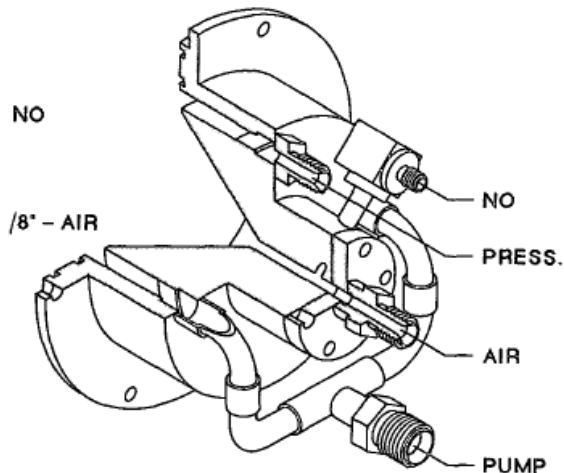


Figure 3: This depicts the conical reaction chamber, the region where NO is entered, where the ambient air is pulled in, and where the pump is located [Ridley *et al.*, 1991].

d. Measurement of aerosols via the aerodynamic particle sizer and micro-orifice deposit impactor

A total aerosol sampler (TAS) and a micro-orifice impactor (MOI) are utilized to collect dust and pollution aerosols for ion chromatographic analysis. An aerodynamic particle sizer (APS) is used to estimate the total coarse-mode volume. A differential mobility analyzer separates molecules based on their electron mobility.

1) INLET

The LTI (low turbulence inlet) uses a porous diffuser to minimize turbulence and its associated losses of large particles [Kline *et al.*, 2004]. This makes it possible to compute the relationship between ambient and sampled coarse aerosol distributions [Kline *et al.*, 2004]. This inlet tends to enhance large particle concentrations. However, with knowledge of the inlet efficiency and passing efficiency of the tubing connecting the inlet to the sampler, reliable connections can be applied [Kline *et al.*, 2004]. The flow from this inlet then will be split for two analysis processes which include the MOI and the APS.

The inlet makes use of boundary layer suction in a porous diffuser to slow the sample airflow from aircraft air speeds near 150 m/s to velocities near 5 m/s without generating turbulence

[Wilson *et al.*, 2004]. The schematic for the inlet is shown in Figure 4. This suction inhibits the formation of the boundary layer and the generation of turbulence. Venturi pumps (a type of vacuum pumps located outside the aircraft) supply the suction flow and the sample flow [Wilson *et al.*, 2004]. The sample flow and suction flow are returned to the aircraft through a strut. The decrease of turbulence reduces losses of supermicron particles by turbulent deposition and permits the use of laminar flow calculation and drag formulations to accurately predict particle motion [Wilson *et al.*, 2004]. The slowing is critical because high-speed flows in aerosol distribution systems lead to turbulent and inertial losses of large particles [Wilson *et al.*, 2004].

Flow into the LTI enters from the left and the sample airflow leaves the diffuser between the axis and the wall on the right side of the figure [Wilson *et al.*, 2004]. The airflow enters the inlet which is aligned as closely as possible with the local wind vector in order to reduce separation at the leading edge [Wilson *et al.*, 2004]. The leading edge of the inlet is elliptical in shape which permits the inlet to function when the alignment between the local wind vector and the inlet diffuser axis which vary during a research flight. The turbulence reduction is achieved through boundary layer suction in the diffuser.

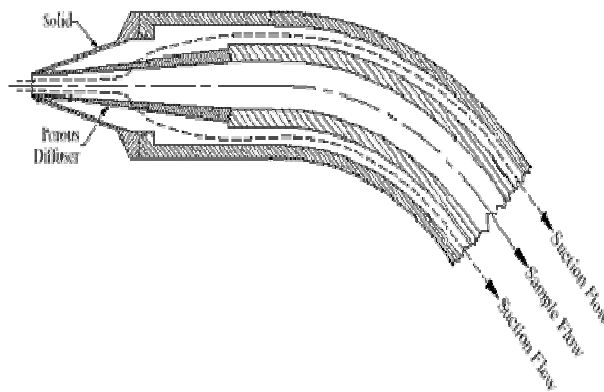


Figure 4: This depicts the Low Turbulence Inlet [Mullen, Jo, 2002].

2) TECHNIQUE

(i) *Technique for Aerodynamic Particle Sizer*

The aerodynamic particle sizer (APS) samples air entering the NCAR/NSF C-130 via an LTI. It is used to size and count particles according to their aerodynamic diameter which is defined as the equivalent settling velocity diameter [Baron, 1986]. The instrument sizes particles aerodynamically by time-of-flight and optically by light scattering intensity [Armendariz, 2002]. It is used to determine the concentration and size distribution of particles from 0.3 to 20 μm in diameter [Armendariz, 2002]. The schematic for the APS is depicted in Figure 5.

The APS accelerates the aerosol particles through a nozzle and passes it through a center of two laser beams [Baron, 1986]. In the nozzle, the particles accelerate through an orifice before recombining with the filtered airflow [Armendariz, 2002]. The aerosol is brought into the inlet

as a sample airflow, part of which is slowed and part of which is filtered [Baron, 1986]. A certain amount of sheath air is allowed to enter. Particles in the nozzle lag behind the air velocity and the difference in velocity between the air and particles is linked to the aerodynamic diameter of the particles. The velocity of particles in reference to the air in the nozzle can attain approximately one third of the speed of sound [Baron, 1986].

The APS measures the particle time of flight between two laser beams and produces pulses for each particle [Baron, 1986]. The intersection of the two laser beams with the particle path defines the detection volume [Baron, 1986]. The light scattering intensity is measured by analysis of the magnitudes of the pulses of scattered light from the lasers [Armendariz, 2002]. The time for each particle to pass between a pair of overlapping laser beams is detected and converted to aerodynamic particle size using a pre-programmed calibration [Armendariz, 2002].

Inaccurate sizing of liquid particles can result from particle deformation in the accelerating inlet gas system [Armendariz, 2002]. In particular, aerodynamic size distribution shows a substantial number of artificial large particles that distorted the distribution and produced false mass median aerodynamic diameters [Stein *et al.*, 2000]. In a study of APS efficiency, it was apparent that some aerosol particles scattered less light than they should based on their apparent aerodynamic diameter which were caused by the slow recirculation of particles through the sensor path [Kline *et al.*, 2004].

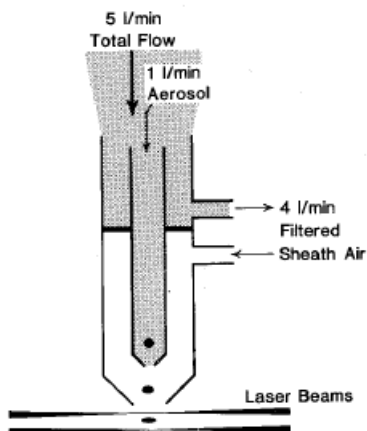


Figure 5: Baron, 1986.

(ii) *Technique for the micro-orifice deposit impactor*

MOUDI is a cascade impactor used to measure size-segregated aerosol chemistry. Air to be sampled by the MOUDI enters through an LTI. It utilizes small nozzle diameters which allow for particles to be collected on the last stage of the impactor [Marple *et al.*, 1986]. By rotating the impaction plates relative to the nozzle plates, homogeneous deposits can be attained on the impaction plates [Marple *et al.*, 1986]. Each stage body of the impactor supports the impactor plate for the stage above and the nozzle plate for the stage below [Marple *et al.*, 1986]. At each stage, jets of particle air are imposed upon an impaction plate and particles larger than the cut

size of each stage are collected on impaction plates. Smaller particles with less inertia follow the air streamlines and proceed onto the next stage. The nozzles of each succeeding stage are smaller than the prior stage. Such gives a higher velocity for the particles through the nozzles and a smaller particle size cut. The airflow continues through a series of impactor stages until the smallest particles are removed by the after-filter.

The impaction plates are rotated relative to the nozzle plate by rotating the stage bodies and holding the other stages in a stationary position [Marple *et al.*, 1986]. Rotation of the alternate stage bodies is accomplished by gears on these bodies that mesh with gears on an electrically driven drive shaft of a rotating mechanism [Marple *et al.*, 1986]. The alternate stage bodies are restrained from rotation by pins that rest on the drive shaft. Particles can be collected on an annular foil impaction substrate that can be placed on the same impaction plate holding the crystal [Marple *et al.*, 1986]. By using a combination of two surfaces (i.e. crystal and an annular foil) as the two substrates, it is possible to calibrate the one of the surfaces directly for the detection of particles [Marple *et al.*, 1986].

There is also often a gas denuder which is attached to an inlet used to remove gases which may disturb the interpretation with the utilization of parallel plates/ strips such as nitric acid and organic vapor [DRI, 1992]. The samples collected are analyzed by ion chromatography as described for the process of analysis for the total aerosol sampler.

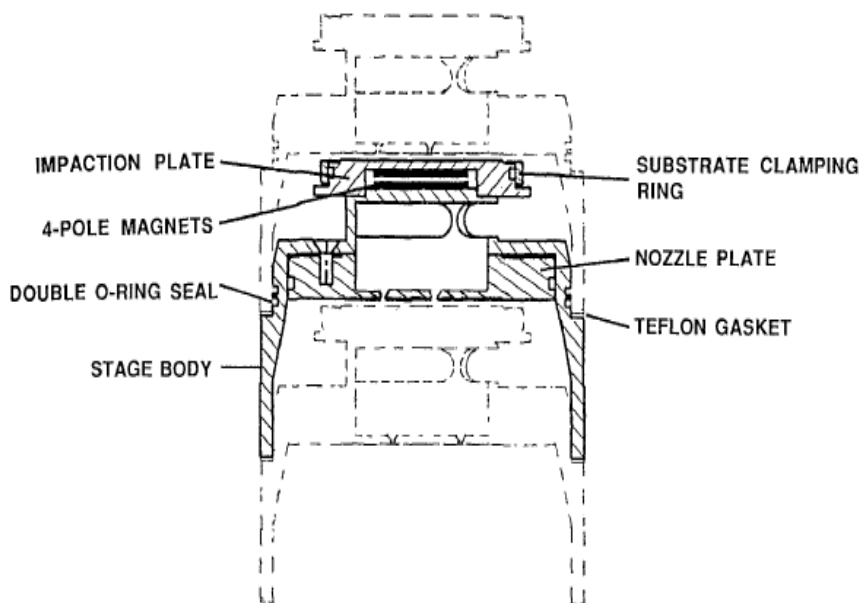


Figure 6: This figure depicts the MOUDI (Micro-orifice uniform deposit impactor) [Marple *et al.*, 1986]. It consists of a nozzle plate, impaction plate, substrate clamping ring, stage body, and 4-pole magnets [DRI, 1992]. The nozzle plate is a metal plate with 10-2,000 nozzles machined by computerized drilling [DRI, 1992]. The impaction plate is magnetically secured by the 4-pole magnets on top of each impact stage and serves to collect particles from nozzle jets from stage above [DRI, 1992]. The rotator stage is a device for rotating the impactor stages to provide the uniform deposit [DRI, 1992].

e. Measurement of aerosols via differential mobility analysis

1. INLET

The solid diffuser inlet was designed by Dr. Anthony Clarke and previously used aboard the PEM-Tropics A & B campaigns [McNaughton *et al.*, 2007]. In this case it functions to draw air in for the differential mobility analysis.

The inlet is designed for a nominal volumetric flow rate of 100 lpm (liters per minute) and features a shrouded constant-area flow region around the inlet; a 4.5-degree diffuser half-angle and a 3.8 cm inner diameter tube with the a large possible radius of curvature for the inlet to complete a 45 degree bend to bring the air into the fuselage [McNaughton *et al.*, 2007]. The schematic for the inlet is shown in Figure 7. The inlet tip has a minimum diameter of 5.13 mm with a double elliptical leading edge to reduce flow separation (0.25 mm) [McNaughton *et al.*, 2007]. The inlet is tilted at a small angle to facilitate iso-axial sampling [McNaughton *et al.*, 2007]. Under some conditions a fraction of large dust particles may not be retained when they impact on inlet and tubing walls [Huebert *et al.*, 2004].

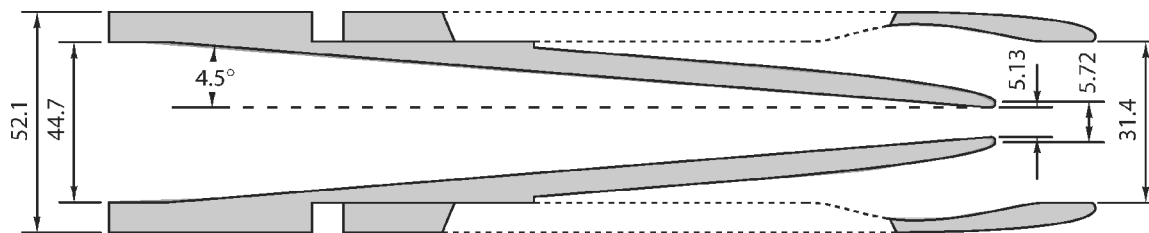


Figure 7: Hubert *et al.*, 2004, PELTI.

2. TECHNIQUE

The differential mobility analyzer is used for electrostatic analysis of polydisperse aerosols [Adachi *et al.*, 2007]. It is utilized both as an aerosol sizing instrument as well as a monodisperse aerosol generator of particles less than 1 mm in diameter [Adachi *et al.*, 2007].

After bipolar charging in a neutralizer which generates a high level of positive and negative ions, the aerosol is introduced into the DMA [Adachi *et al.*, 2007]. Specifically, the neutralizer brings the aerosol charge level to an equilibrium charge distribution which leads to the individual aerosol particles acquiring either a single positive, single negative, or a zero charge. The DMA separates particles based on their electrical mobility [Hagwood, 2001]. At the inlet slit, aerosol particles are injected into the annular region between the two cylinders [Hagwood, 2001]. They are transported by clean air flowing through the annular region [Hagwood, 2001]. Particles with velocities in a certain narrow range are sampled at the sampling slit. Then, the size distribution is inferred via an inversion calculation [Hagwood, 2001]. The sizing is a function of adjustable parameters such as voltage, flow rates, etc. For sizing nanometer particles, Brownian motion (random motion of microscopic molecules) becomes important [Hagwood, 2001].

f. Measurement of aerosols via total aerosol sampler

This total aerosol sampler (TAS) does not have an inlet for collection of aerosol particles which thus excludes any losses associated with the transportation of the particles. Instead, the total aerosol sampler consists of a cone diffuser liner and a filter or each sample and then replaced [Kline et al., 2004].

The TAS sampler is designed so that every particle entering its tip can be extracted and analyzed [Huebert et al., 2002]. All particles inflowing TAS will be either collected on the filter or deposited to the inner walls of the cone so that no particle will be lost [Huebert et al., 2002]. A different cone liner and a filter are used for each sample [Kline et al., 2004].

The removable cones that line the diffuser are about 150 mm in length with an inlet orifice of about 6 mm diameter and an exit of just over 74 mm diameter [Huebert et al., 2002]. The exit opening is designed to sit tightly against a 90 mm Teflon filter [Huebert et al., 2002]. The cones are coated with Teflon to minimize the collection of acidic gases (nitric acid). The external tip of the structure that holds the removable cones was sized to allow for isokinetic sampling at a range of C-130 airspeeds [Huebert et al., 2002].

At the end of the flight, all the filters and cone liners are separately extracted. The separate extraction of the interior of the cone and the filter and the subsequent division of the mass of each analyte by the volume of air sampled allows for an ambient bulk calculation to be derived [Huebert et al., 2002]. For identification of analytes collected, ion chromatography is used which implements 2 Dione Ion Chromatographs. This process involves separating the particles by their electron mobility via the particles' interaction with an absorbing type of material.

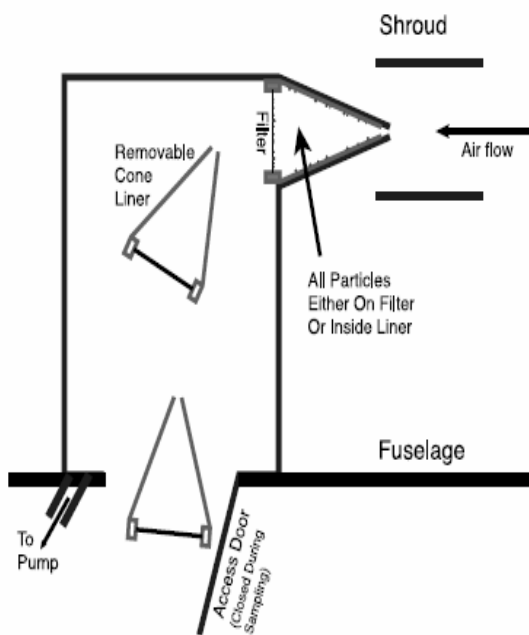


Figure 8: [Kline et al., 2004]

g. Measurement of cloud condensation nuclei

1) INLET

The inlet for CCN measurements is not highly specialized as the transportation of CCN is less complicated. In particular, for small particles smaller than approximately 100 nm (i.e. sea salt or ammonium sulfate), sampling is simple as such particles react quickly and can follow air streamlines. For particles larger than 500 nm, the aerosols are in an aqueous solution (i.e. sulfuric acid) which makes the sampling more complicated. As for inlets used in other sampling techniques, wall losses can also be significant. However, they can be corrected with the knowledge of particle size and mass density, air flow rate through inlet, speed of aircraft, and bend radius of the inlet.

The particle airflow is set to approximately $100 \text{ cm}^3\text{s}^{-1}$ by a mass flow controller [Hudson, 1989]. A particle-free filtered air that surrounds the sample flow is made laminar as it passes between plates because it is forced through 100's of holes in a plastic block [Hudson, 1989]. It is necessary for the filtered flow which will be surrounding the sample airflow to be nonturbulent in order to minimize the reaction of the particles going through the thermal diffusion chamber with the walls. Significant higher airflows dry the chamber and thus do not give enough time for sufficient droplet growth while significant lower flows result in the precipitation of some droplets to the bottom of the thermal diffusion chamber [Hudson, 1989].

The chamber operates at a pressure below ambient so that the sample can be sucked in by a pressure difference. This is because the sample air flow cannot be directly controlled as such a process requires a flow controller which would manipulate the flow as a function of altitude [Hudson, 1989]. It is operated at about 300 mb [Hudson, 1989]. Another reason why the pressure needs to be controlled in such a way is in order to maintain the droplet growth rate [Hudson, 1989]. The constant volume flow through the thermal diffusion chamber will allow the droplets to grow an equivalent amount of time [Hudson, 1989].

2) TECHNIQUE

CCN measurements are made with a thermal gradient diffusion cloud chamber which produces a CCN spectrum over a range from 0.01% to 1% supersaturation values. It utilizes a supersaturation field that increases along the path of the flow of sample [Hudson, 1989]. The schematic for this instrument is depicted in Figure 9.

The thermal diffusion chamber utilizes several zones of increasing supersaturation [Hudson, 1989]. A row of thermoelectric modules maintains the temperature of each side is [Hudson, 1989]. The thermoelectrics either cool or heat the plates as necessary in order to maintain the temperature of each supersaturation zone [Hudson, 1989]. The increasing supersaturation field allows the lower S_c nuclei to begin growing earlier and to continue to have a greater driving force for growth and thus maintain a greater size than the higher S_c nuclei which are only activated to cloud droplet growth in later stages of the cloud chamber [Hudson, 1989]. Thus the droplet size is inversely correlated to the S_c . The distilled water is fed by gravity to a foam rubber strip which is squeezed between 2 plates [Hudson, 1989]. Some of the

water is evaporated from each plate to humidify the air and grow droplets; the excess flows down sides of the two plates and out the holes into a reservoir [Hudson, 1989].

Each droplet passes individually through a white light beam that intersects the particle beam from the cloud chamber [Hudson, 1989]. A pmt detects the scattered light and generates a pulse proportional to the size of the particle [Hudson, 1989]. The CCN spectrum is derived from the final droplet size distribution which has been determined to be related to the nucleus critical supersaturation based on routine calibrations [Hudson, 1989]. This procedure relies on the calibration of instrument with particles with a specified critical supersaturation (S_c) [Hudson, 1989].

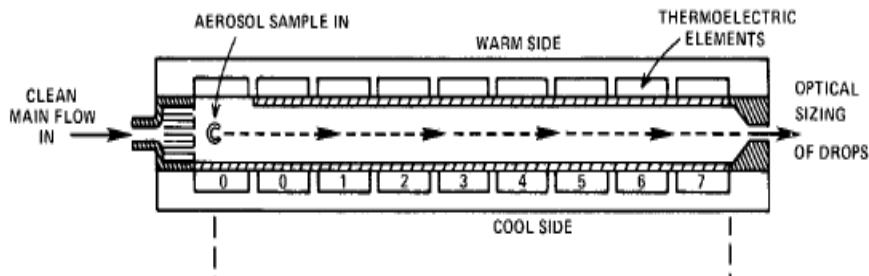


Figure 9: Hudson, 1989.

h. Special Specifications for the C-130

1. RACKS

There are also 8 instrumentation racks for instruments which have been specifically engineered to withstand overturning. Thus, for each individual instrument part, an overturning arm had to be calculated to be 16,200 lb-in. Each rack is also engineered to withstand emergency landing loads and in-flight gust loads. The in-flight gust loads are loads resulting from turbulence and are 8.25 g down and 5.25 g up (i.e. 100 lb will have to withstand 825 pounds) [Lord, 2002]. The emergency landing loads are defined as the loading that occurs during other than a normal landing: wheels-up loading or veering off the runway which include 9g forward, 3g up, 6g down, 3g side, and 1.5g aft [Lord, 2002]. The maximum payload of the aircraft is 23,000 lb.

2. SPECIALIZED INSTRUMENTATION

In addition to the instrumentation described for measurements of atmospheric gases, aerosols, and cloud condensation nuclei, C-130 is equipped with the following sensors: atmospheric state parameters, gustprobe instrumentation for turbulent flux measurements, cloud physics instrumentation, radiometers (short and longwave, ultraviolet, and multi-channel scanning shortwave, imaging microwave radiometer, remote radiometric surface temperature, video photography, dropwindsonde dispensing acquisition, oceanographic dropsonde dispensing, electric field strength sensing, aerosol lidar [RAF, 2005].

In the nose section, a radome differential gust probe system is situated. It will sense wind vector horizontal component, wind vector vertical component, and a horizontal wind direction [RAF, 2003]. The wind components can be used to determine turbulent fluxes. It will also house a laser spectrometer which will take an aerosol spectrum, cloud droplet spectrum (0.5 to 47 μm , 0.3 to 200 μm , 40 to 620 μm), a hydrometer spectrum (300-4500 μm , 25-800 μm), and a cloud particle spectrum (25-800 μm) [RAF, 2003]. In addition, the instrument will also measure angle of attack (flow angle sensor, radome) with a range of $\pm 10^\circ$ and an accuracy of $\pm 0.134^\circ$, angle of sideslip (flow angle sensor, radome) with a range of $\pm 5^\circ$ and an accuracy of $\pm 0.096^\circ$ [RAF, 2003].

Various profiles of radiation fluxes will also be measured. Radiometric surface temperature is measured with a bolometric radiometer with a range of -50 to 60°C and an accuracy of $\pm 0.5^\circ\text{C}$, IR radiation pyrgometer which measures in the range 3.5 to 50 μM with a range of 0 – 600 W/m^2 , visible radiation measured with a 0.285-2.8 μM with a range of 0-1500 W/m^2 , and UV radiation which is measured via a photometer in the wavelengths 0.295 to 0.385 μM in the range of 0-200 W/m^2 [RAF, 2003].

A thermoelectric hygrometer measures dew-point temperature from -65 to 50°C with an accuracy of $\pm 0.5^\circ\text{C}$ (temperature $> 0^\circ\text{C}$) and an accuracy of $\pm 1^\circ\text{C}$ (temperatures of $< 0^\circ\text{C}$); deiced platinum resistance and platinum resistance provide total air temperature from -60 to +40°C with an accuracy of $\pm 1^\circ\text{C}$; variable capacitance provides airspeed pressure from 0-125 mb with an accuracy of ± 0.7 mb; variable capacitance and oscillation frequency provides fuselage static pressure from 250-1035 mbar with an accuracy of ± 1 mb [RAF, 2003].

The inertial navigation system provides aircraft roll angle, pitch angle, aircraft pitch angle, true heading, vertical velocity, ground speed, longitude, and longitude [RAF, 2003]. The C-band Doppler radar will display areas of turbulence, reflectivity, or a combination of the two.

3. Results and Discussion

The following data (Figures 10 and 11) are taken from 31 July, 2007 Test Flight. It includes the measurements for OH, H₂SO₄, MSA, HO₂, and HO₂+RO₂. Measurements for NH₃ were not available as the mass analyzer and channeltron were not tuned up to select the specific masses of the NH₄⁺ ions.

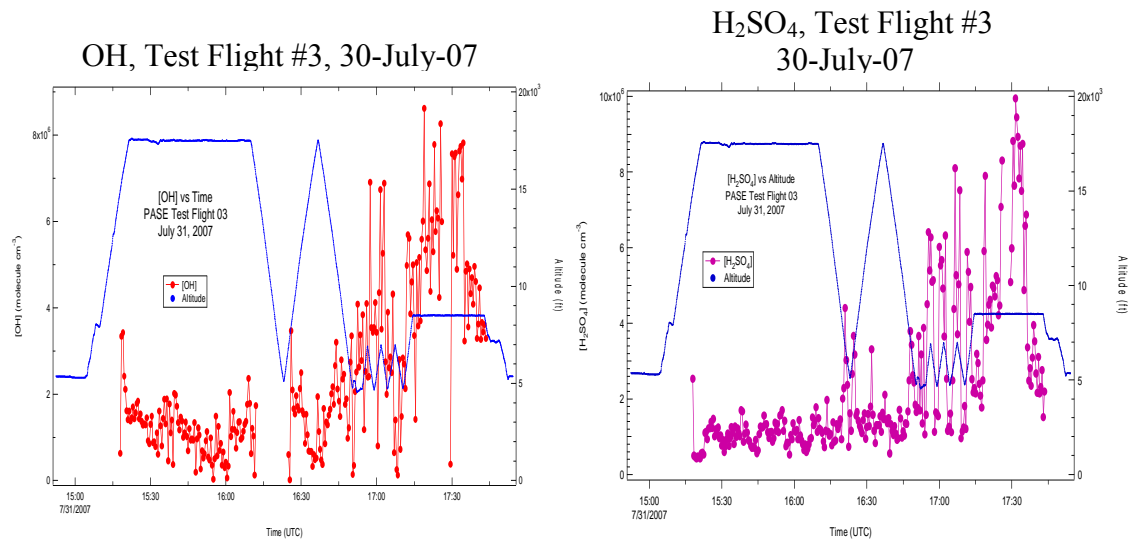


Figure 10: (a) OH measurements from Test Flight #3 (b) H₂SO₄ measurements from Test Flight #3.

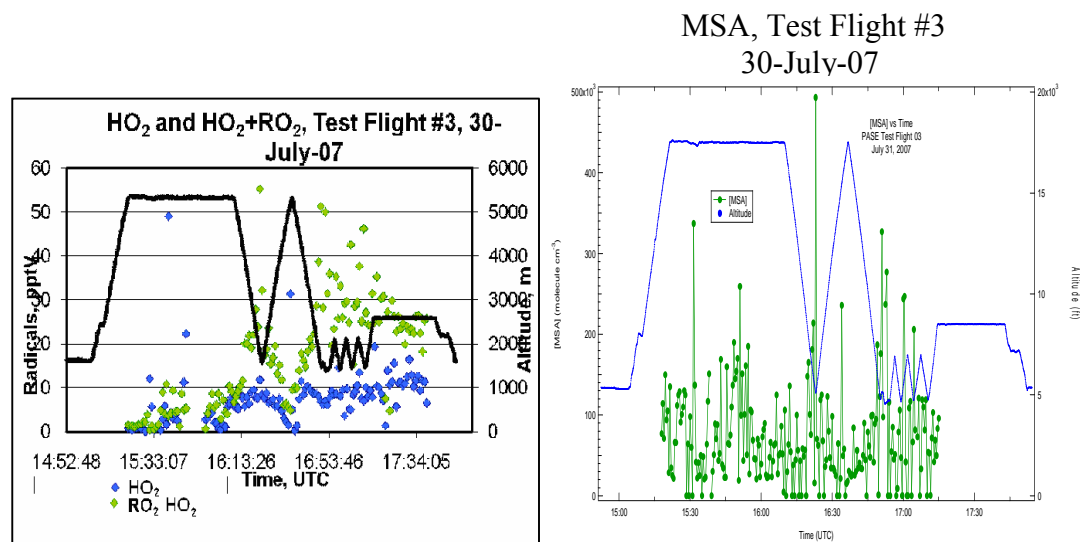


Figure 11: (a) HO₂, HO₂+RO₂ measurements from Test Flight #3 (b) MSA measurements from Test Flight #3

Presented in the Figure 10(a) is OH variability and an altitude profile for that particular flight. It can be clearly seen that at lower altitudes, the OH concentrations increase and at higher altitudes, OH concentrations decrease. This variability occurs due to the presence of water vapor, which is a limiting reagent at higher altitudes. The smaller scale structure occurs by changes in O₃ and NO [Mauldin *et al.*, 1998]. Spikes of OH were presumably due to brief occurrences of elevated NO concentrations [Mauldin *et al.*, 1998]. It can be seen in Figure 10(b) that H₂SO₄ variability follows the OH variability which is because OH is the primary oxidation agent of SO₂ in the atmosphere which leads to formation of H₂SO₄.

Similar to the OH and H₂SO₄ concentrations, HO₂ and HO₂+RO₂ concentrations in Figure 11(a) also vary similarly with height as water vapor is also a limiting reagent in their formation. The larger concentration of HO₂+RO₂ than the HO₂ needs more investigation. It has been proposed previously that the concentration of these two radicals is largely controlled by their interaction with OH and aerosols [Cantrell *et al.*, 1996].

Also presented here in Figure 11(b) are the MSA concentrations which are extremely low. The primary reason for this is that MSA results from the oxidation of DMS from phytoplankton and thus continental atmosphere will have limited amount of this particular gas. However, several peaks in the MSA are clearly visible. A possible explanation for this could be some marine air was transported at high altitude and the particles in it evaporated releasing MSA into the air.

4. Conclusion:

The Pacific Sulfur Atmospheric Experiment field campaign employs the utilization of aircraft for specific airborne measurements in order to understand the sulfur cycle in a remote marine atmosphere also known as the CLAW hypothesis.

Aircraft measurements have inherent constraints such as the limitations on the instrument payload which include their size, weight, and power. Atmospheric measurements also must be made rapidly while taking into account the changing pressure, temperature, and relative humidity. Such measurements also suffer from biases that result from modifications occurring in the sampling system that brings atmospheric particles to the instrument. This paper described the design of the inlets and the instruments utilized and situated aboard the C-130 with a focus on how some of the constraints have been overcome and which still remain to be such for the SICIMS, APIMS, TSA, MOUDI, APS, DMA, CCN counter, O₃ slow and fast response instruments.

With respect to sample measurements during the test flight, the dependency of OH, H₂SO₄, HO₂, and HO₂+RO₂ concentrations on water vapor are shown. Also show certain peaks from MSA which could be present as a result of transportation of marine air at higher altitudes. Measurements also indicate the higher concentrations of measurements from the SICIMS in the HO₂+RO₂ mode relative to the HO₂. Both of these results require future research.

My participation in the PASE campaign from 14 -21 August, 2007 will include participation in observing the operation of the SICIMS instrument and using it to take measurements of hydroxyl, sulfuric acid, methane sulfonic acid, ammonia, and peroxy radicals.

ACKNOWLEDGMENT

The author would like to thank Lee Mauldin for putting the final paper together; Rebecca Anderson for multiple reviews of the sampling techniques and measurements of peroxy radicals; Illana Pollack for providing information on the technique used for ozone measurements; Byron Blomquist for providing information on the technique used for DMS, DMSO, DMSO₂, and SO₂

measurements; Dave Rogers and Jim Hudson for providing information on the technique and sample measurements of cloud condensation nuclei; Mark Lord for providing general information on C-130.

REFERENCES

- Adachi, Motoaki, Kikuo Okuyama, Yasuo Kousaka, Seong Won Moon, John H. Seinfeld, 2007: Facilitated Aerosol Sizing Using the Differential Mobility Analyzer. *Aerosol Sci. Technol.*, **12**, 255-239.
- Armendariz, Alfredo J., David Leith, 2002: Concentration measurement and counting efficiency for the aerodynamic particle sizer 3320. *Aerosol Sci. Technol.*, **33**, 133-148.
- Aisawa, Edward, Bertsch, James L.; J. Michael Flanagan; Darrell L. Gourley. Ionization chamber and mass spectrometer having a corona needle which is externally removable from a closed ionization chamber. U.S. Patent 5,726, 447. March 10, 1998.
- Bandy, Alan R., Donald C. Thornton, Fang H. Tu, Byron Blomquist, Wolfgang Nadler, and Glenn M. Mitchell, 2002: Determination of the vertical flux of dimethyl sulfide by eddy correlation and atmospheric pressure ionization mass spectrometry. *J. Geophys. Res.*, **107**, 4743-4752.
- Bandy, Alan, 2006: Feasibility Analysis: Pacific Atmospheric Sulfur Experiment, Drexel University.
- Baron, Paul A., 1986: Calibration and Use of the Aerodynamic Particle Sizer. *Aerosol Sci. Technol.*, **5**, 55-67.
- Cantrell, C.A., R.E. Shetter, T.M. Gilpin, J. G. Calvert, F.L. Eisele, and D.J. Tanner, 1996: Peroxy radical concentrations measured and calculated from trace gas measurements in the Mauna Loa Observatory Photochemistry Experiment 2. *J. Geophys. Res.*, **101**, 14,653-14,664.
- Cantrell, C.A., A. Zimmer, and G. Tyndall, 1997: Absorption cross section for water vapor from 183 to 193 nm. *Geophys. Res. Lett.*, **24**, 2195-2198.
- Charlson R., J. Lovelock, M. Andreae and S. Warren, 1987: Oceanic phytoplankton, atmospheric sulphur, cloud albedo and climate. *Nature*, **326**, 655-661.
- Desert Research Institute, 1992: Standard Operating Procedure for Routine Operation of the Micro-Orifice Uniform Deposit Impactor (MOUDI) in CRPAQS. <http://www.arb.ca.gov/airways/crpaqs/STI/AppA18.pdf> (accessed August 2, 2007).
- Edwards, Gavin D., Christopher A. Cantrell, Sherry Stephens, Brian Hill, Olusegun Goyea, Richard E. Shetter, R. Leon Mauldin, III, Edward Kosciuch, David J. Tanner, and Fred L. Eisele, 2003: Chemical ionization mass spectrometer instrument for the measurement of tropospheric HO₂ and RO₂. *Anal. Chem.*, **75** (20), 5317 - 5327.
- Eisele, F.L., D.J. Tanner, 1991: Ion-assisted tropospheric OH Measurements, *J. Geophys. Res.*, **96**, 9295-9308.
- Eisele, F.L., R.L. Mauldin III, D.J. Tanner, J.R. Fox, T. Mouch, and T. Scully, 1997: An inlet/sampling duct for airborne OH and sulfuric acid measurements. *J. Geophys. Res.*, **102**, 27,993-28,001.
- Hagwood, Charles, Statistical Engineering Division, School of Mechanical Engineering, Purdue University, 2001: 3.3.2 Understanding the Differential Mobility Analyzer. <http://www.itl.nist.gov/div898/pubs/ar/ar11996/node28.html> (accessed August 2, 2007).
- Hudson, James G., 1989: An Instantaneous CCN Spectrometer. *J. Atmos. Ocean Technol.*, **6**, 1055-1065.
- Huebert, Barry, Timothy Bertram, Jena Kline, and Steven Howell, 2004: Measurements of organic and elemental carbon in Asian outflow during ACE-Asia from the NSF/NCAR 130. *J. Geophys. Res.*, **109**, D19S11, doi:10.1029/2004JD004700.
- Huebert, Barry J., Steven G. Howell, David Covert, Timothy Bertram, Anthony Clarke, James R. Anderson, Bernard G. Lafleur, W.R. Seebaugh, James Charles Wilson, Dave Gesler, Byron Blomquist, and Jack Fox, 2004: PELTI: Measuring the Passing Efficiency of an Airborn Low Turbulence Inlet. *Aerosol Sci. Technol.*, **38**, 803-826.
- Huebert, Barry, Department of Oceanography, University of Hawaii: Aircraft C-130 Bulk Aerosol Mass of Anions and Cations from TAS. http://data.eol.ucar.edu/codiac_data/ace-asia/docs/TASHuebertReadme.html (accessed August 2, 2007).
- Kline, J., B. Huebert, S. Howell, B. Blomquist, J. Zhuang, T. Bertram, and J. Carrillo, 2004: Aerosol composition and size versus altitude measured from the C-130 during ACE-Asia. *J. Geophys. Res.*, **109**, D19S08, doi: 10.1029/2004JD004540.

- Kline, J., B. Huebert, S. Howell, B. Blomquist, J. Zhuang, T. Bertram, and J. Carrillo, 2004: Aerosol composition and size versus altitude measured from the C-130 during ACE-Asia. *J. Geophys. Res.*, **109**, D19S08, doi: 10.1029/2004JD004540.
- Krupa, S.V., Effects of atmospheric ammonia (NH₃) on terrestrial vegetation, 2003: a Review, *Environmental Pollution*. **124**, 179-221.
- Kuhlmeier, Gregory A., Benjamin Y. H. Liu, Virgil A. Marple, 2007: A micro-orifice impactor for sub-micron aerosol size classification. *American Industrial Hygiene Association Journal*, **42**, 790-795.
- Kulmala, M., M. Dal Maso, J.M. Makela, L. Pirjola, M. Vakeva, P. Aalto, P. Mikkilainen, K. Hameri, and C.D. O'Dowd, 2000: On the formation, growth and composition of nucleation mode particles. *Tellus B*, **53**, 479-490.
- Kulmala, M., P. Korhonen, I. Napari, A. Karlsson, H. Berresheim, and C.D. O'Dowd, 2001: Aerosol formation during PARFORCE: Ternary nucleation of H₂SO₄, NH₃, and H₂O. *J. Geophys. Res.*, **107**(D19), 8111.
- Kukui, Alexander, Dmitri Borissenko, Gerard Laverdt, and Georges Le Bras, 2003, Gas-Phase Reactions of OH Radicals with Dimethyl Sulfoxide and Methane Sulfonic Acid Using Turbulent Flow Reactor and Chemical Ionization Mass Spectrometry. *J. Phys. Chem.*, **107**, 5732-5742.
- Lelieveld, J., F.J. Dentener, W. Peters, and M.C. Krol, On the role of hydroxyl radicals in the self-cleansing capacity of the troposphere. *Atmos. Chem. Phys.*, **4**, 2337-2344.
- Lenggoro, Wuled, Bin Xia, and Kikuo Okuyama, 2002: Sizing of Colloidal Nanoparticles by Electrospray and Differential Mobility Analyzer Methods. *Langmuir*, **18**, 4583-4591.
- Lord, Mark, Research Aviation Facility, Earth Observing Laboratory, University Corporation for Atmospheric Research, 2002: Bulletin No. 13: Design, Fabrication, and Approval of User-Supplied Equipment for NSF/NCAR. <http://www.eol.ucar.edu/raf/Bulletins/bulletin13.html> (accessed August 2, 2007).
- Mauldin, R.L., III, G.H. Frost, G. Chen, D.J. Tanner, A.S.H. Prevot, D.D. Davis, and F.L. Eisele, 1998: OH measurements during the First Aerosol Characterization Experiment (ACE 1): Observations and model comparisons. *J. Geophys. Res.*, **70**, 16,713-16,729.
- Marple, V., K. Robow, G. Annanth, and H.J. Fissan, Micro-orifice uniform deposit impactor. *J. Aerosol Sci.*, **17**, 3, 489-494.
- McNaughton, Cameron S., Antony D. Clarke, Steven G. Howell, Mitchell Pinkerton, Bruce Anderson, Lee THornhill, Charlie Hudgins, Edward Winstead, Jack E. Dibb, Eric Scauer, and Hal Maring, 2007: Results from the DC-8 Inlet Characterization Experiment (DICE): Airborne Versus Surface Sampling of Mineral Dust and Sea Salt Aerosols. *Aerosol Sci. Technol.*, **41**, 136-159.
- Mullen, Jo, Department of Engineering, University of Denver, 2002: The Low Turbulence Inlet – Concept. http://www.engr.du.edu/aerosol/lti_concept.htm (accessed August 2, 2007).
- Pollack, Illana, Personal Communication, 2007: HIAPER Instrumentation: A Proposal to Develop In Situ Ozone Instruments (July 30, 2007).
- Profitt, Michael H., Richard J. McLaughlin, 1993: Fast-response dual-beam UV-absorption ozone photometer suitable for use on stratospheric balloons. *Rev. Sci. Instr.*, **54**, 1719-1728.
- Research Aviation Facility, Earth Observing Laboratory, University Corporation for Atmospheric Research, 2003: Bulletin No. 3: The NSF/NCAR C-130Q Hercules Overview and Summary of Capabilities. <http://www.eol.ucar.edu/raf/Bulletins/bulletin3.html> (accessed August 2, 2007).
- Research Aviation Facility, Earth Observing Laboratory, University Corporation for Atmospheric Research, 2005: Preliminary Specification: EC-130Q Hercules. <http://www.eol.ucar.edu/raf/Aircraft/c130.html> (accessed August 2, 2007).
- Ridley, B.A., F.E. Grahek, and J.G. Walega, 1991: A small, High-Sensitivity, Medium-Response Ozone Detector Suitable for Measurements from Light Aircraft. *J. Atmos. Ocean Technol.*, **9**, 142-148.
- Röttgen, Martin A., Ken Judal, Jean-Marie Antonietti, Ueli Heiz, Stephan Rauschenbach, and Klaus Kern, 2006: Conical octopole ion guide: design, focusing, and its application to the deposition of low energetic clusters. *Rev. Sci. Instr.*, **77**, 013302.
- Schanot, Allen, Research Aviation Facility, Earth Observing Laboratory, University Corporation for Atmospheric Research, 2002: New Capabilities for the C-130Q Hercules. http://www.eol.ucar.edu/raf/new_cap_C130.html (accessed August 2, 2007).
- Schwartz, S. E., The whitehouse effect – Shortwave radiative forcing of climate by anthropogenic aerosols, 1996: An overview. *J. Aerosol Sci.*, **27**, 359-382.
- Shukla, Anil K., Jean H. Futrell, 2000: Tandem mass spectrometry: dissociation of ions by collisional activation. *J. Mass Spectrom.*, **35**, 1069-1090.

- Tanner, D.J., A. Jefferson, and F.L. Eisele, 1997: Selected ion chemical ionization mass spectrometric measurement of OH. *J. Geophys. Res.*, **102**, 6415-6425.
- Thomas, Robert, 2001: A Beginner's Guide to ICP-MS Part V: The Ion Focusing System. *Spectroscopy*, **16(9)**, 38-44.
- Thornton, Donald C., Alan R. Bandy, Fang H. Tu, Byron Blomquist, Glenn M. Mitchell, and Wolfgang Nadler, 2002: Fast airborne sulfur dioxide measurements by Atmospheric Pressure Ionization Mass Spectrometry. *J. Geophys. Res.*, **109**, 4,632-4,644.
- Wang, Jian, Richard C. Flagan, and John H. Seinfeld, 2003: A differential mobility analyzer (DMA) System for Submicron Aerosol Measurement at Ambient Relative Humidity, *Aerosol Sci. Technol.*, **37**, 46-52.
- Wilson, J.C., B.G. Lafleur, H. Hilbert, W.R. Seebaugh, J. Fox, D.W. Gesler, C.A. Brock, B.J. Huebert, and J. Mullen, 2004: Function and Performance of a Low Turbulence Inlet for Sampling Supermicron Particles from Aircraft Platforms. *Aerosol Sci. Technol.*, **38**, 790-802.

APPENDIX A: Description of Inlets, Technique, Calibration, and Measurements of OH, H₂SO₄, MSA, NH₃, HO₂, HO₂+RO₂

a. Description of Sampling Ducts

The sampling ducts for the three inlet channels share the same function but are different in their structures because of the different chemical properties of gases measured.

The OH, H₂SO₄, and MSA sampling has to be positioned nearly parallel to the flow because transportation of OH and H₂SO₄ has to be relatively quick as these gases have very short lifetimes in the atmosphere. At the same time, the sampling duct must minimize flow separation, straighten the flow and make it nonturbulent which is necessary to keep OH and H₂SO₄ from reacting with other molecules and with the walls of the sampling duct. The two cylindrical ducts located to the rear of the sampling inlet reduce the flow 16 fold from 100-150 m/s to 6-10 m/s [Eisele *et al.*, 1997]. The elliptical surfaces (3:1 for the inside and 4.5:1 outside surface major to minor axis ratios) are used for flow straightening and for minimizing flow separation. The inlet is also positioned for an angle of attack (AOA) of 9 to 10° which would exclude a large amount of precipitation from entering the inlet. The inlet itself is curved, causing the air flow to bend. By bending the sample airflow, the water droplets would hit the walls of the inlet because they would follow straight trajectories. This inlet also functions at ambient pressure. A more thorough description of the inlet can be found in [Eisele *et al.*, 1997]. The air flow is pumped down by the virtual iris, positioned at the end of the drift tube before its entrance into the collisional dissociation chamber which will be discussed later.

The construction of the NH₃ sampling duct is similar to the OH inlet. It also contains two cylindrical ducts located to the rear of the flow necessary for flow reduction. The main difficulty encountered with this measurement is that NH₃ is an extremely sticky molecule as a result of its polar nature and thus often sticks to the walls of the sampling duct. Thus, high speed needs to be maintained. The speed obtained (6-10 m/s), is still fast enough so that the NH₃ molecules coming off the walls would not make it to the pinhole pump located at the rear of the sampling duct. One major difference is that this sampling duct possesses only one set of elliptical surfaces to straighten the flow and minimize its separation. This is because the air flow has to be turbulent in order to make the concentration of NH₃ molecules more evenly distributed. The chemical ionization region of the NH₃ to NH₄⁺ and the pinhole pump that follows it are located to the rear of the sampling duct. The pinhole pump which sucks in the air flow with the ions formed, will be discussed in more detail later.

The HO₂, HO₂+RO₂ inlet is placed orthogonal to the flow and thus reduction of the speed of the air flow is not necessary. The placement of the inlet is such because the peroxy radicals have slightly longer lifetimes and are not as reactive as OH. One main difference is that while the chemical reaction and ionization regions of the NH₃ and OH inlets take place at ambient pressure, this inlet functions at a reduced pressure of 150 Torr. A reduction of pressure in the inlet is necessary because such a condition is more favorable for chemical reaction and ionization to take place.

b. Part 1: Chemical Ionization of OH

The ionization region for the chemical ionization of OH is shown in Figure 1. To measure the OH signal, $^{34}\text{SO}_2$ is injected into the sample airflow (on the order of 10 ppm) in the sample tube by the front injector. It is added in order to discriminate the naturally occurring H_2SO_4 which forms from the naturally occurring OH [Mauldin *et al.*, 1998]. Reactions R12, R13, and R14 describe this neutral chemical process.



HNO_3 is injected by the rear injector and is necessary to eliminate any SO_2 in the airflow so that the OH and the H_2SO_4 measurements won't be amplified. The airflow picks up the HNO_3 molecules (on the order of ppb) as it blows across a small HNO_3 vial at a rate of 2 to 3 sccm. A flow of ambient air is also pulled in from the outside which contains the ambient HNO_3 concentration. This is necessary in order to maintain the $\text{NO}_3 \cdot \text{HNO}_3$ as the primary reactant ion present. The $\text{NO}_3 \cdot \text{HNO}_3$ ion cluster is used because only a small amount of sensitivity is lost by using it in comparison with NO_3^- ions. Whereas, the use of $\text{NO}_3^- (\text{HNO}_3)_2$ ions would reduce the formation of HSO_4^- ions by a factor of 2 [Tanner *et al.*, 1997]. The sample flow then enters the region surrounded by ^{241}Am foil which ionizes the outer coaxial layer of the sheath flow through decay. The ^{241}Am source with an approximate voltage of 5 MeV also acts to minimize ionization of the sample flow and that the initial ionization would be confined to the outer regions of the sheath flow [Mauldin *et al.*, 1998]. Specifically, ^{241}Am is radioactive and through its production of beta particle it will react with nitric acid and knock the hydrogen atom off. In this region, the formation of the $\text{NO}_3 \cdot \text{HNO}_3$ ion clusters takes place (the NO_3^- is ambient and the HNO_3^- formed via passing the ^{241}Am foil). The $\text{H}_2^{34}\text{SO}_4$ is not ionized as these molecules are located at the center of the flow and are protected from ionization by the sheath flow.

These ions are then directed through the intermediate layer of the sheath flow into the central sample flow by the electrostatic lens. The actual $\text{NO}_3 \cdot \text{HNO}_3$ ions generated are moved by electric fields (which only move ions and not radicals and other compounds) from outer sheath gas layer of the ion source where they formed into central sampled airflow [Tanner *et al.*, 1997]. Concentrations of MSA and H_2SO_4 are also present in the airflow. The $\text{NO}_3 \cdot \text{HNO}_3$ ions then react with $\text{H}_2^{34}\text{SO}_4$ to form $\text{H}^{34}\text{SO}_4^-$, with H_2SO_4 to form HSO_4^- , and with MSA to form $(\text{CH}_3)\text{SO}_3^-$. This process is shown in R15, R16, and R17.



As ions reach the end of the reaction region, they are again moved from the region in which they reside into a guided dry N_2 buffer before they enter the CDC through the pinhole [Tanner *et al.*, 1997]. This N_2 buffer gas prevents H_2O molecules in sampled air which contains water molecules from passing through the aperture. If several Torr of H_2O pass through along with sampled ions, the rapid cooling of the airflow which occurs as it expands can result in

hydration of sampled ions [Eisele and Tanner, 1991]. Thus, the ions exit the reaction region but not in the original air flow in which they formed. From the measurements of these concentrations, it is possible to determine the amount of OH in the signal. This reaction series is shown in R15 [Mauldin et al., 1998]. At the end of the reaction region, the core ions are directed by electrostatic lenses through the virtual aperture pinhole and the collisional dissociation chamber (CDC) towards the vacuum [Mauldin et al., 1998]. The voltages on the electrostatic lenses will be either positive to direct the negative ions and negative to direct the positive ions; they will usually be in the magnitude range of 50-120V.

Before the ions enter the pinhole, N₂ is injected via the N₂ buffer. The pinhole acts to control the amount of ions entering the vacuum system and will control the pressure to be at about 100 Torr. Such monitoring is necessary because the pressure will change as the aircraft changes altitudes during flight. The central portion of the pinhole consists of two thin disks placed on top of one another: 0.076 cm thick disk, and a series of 0.038 cm thick wedge shaped pieces [Mauldin et al., 1998]. The wedge shaped pieces allow for pumping on the central portion of the pinhole. Because many of the ions are clustered together in their various airflows, they are directed into the vacuum system in a free expansion of N₂ to minimize clustering.

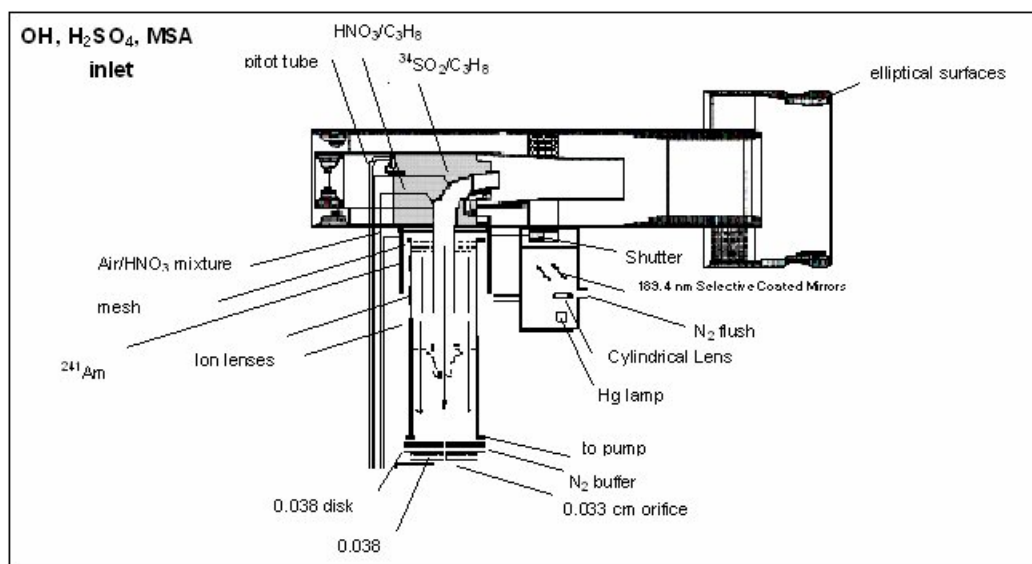


Figure 1: This depicts the OH, H₂SO₄, and MSA inlet.

b. Part 2: Background Measurements of OH

In order to obtain the real measurement of OH, the OH background needs to be subtracted from the OH signal measured in 2.1. Background of OH arises from reactions of HO₂ and RO₂ with NO or O₃. Thus, a mixture of ³⁴SO₂ and propane are added by the first injector. The combination of these two concentrations will leave <2% of OH present. The ³⁴SO₂ will react with ambient OH (R12, R13, and R14). Thus this will measure the ambient OH initially present. Propane is injected through a second pair of injectors (on the order of 10 ppm) to destroy the rest of OH. This is necessary to prevent the cycling of H₂O and RO₂ back into OH

which would add error to the measurements. The $\text{H}_2^{34}\text{SO}_4$ then reacts with NO_3^- (this ion is added using the same technique as during the measurement of the signal) to form $\text{H}^{34}\text{SO}_4^-$ (R15). By measuring $\text{H}^{34}\text{SO}_2^-$ formed, it is possible to determine the amount of the ambient OH (background signal). Measurements of H_2SO_4 and MSA are also done during this time as they do not interfere with the background measurement process.

b. Part 3: Calibration of OH

The instrument for measuring of OH is then calibrated by producing a known amount of OH and measuring it. This is accomplished by photolyzing H_2O with a 184.9 nm emission line from a filtered Hg Pen-Ray lamp (R18) [Mauldin *et al.*, 1998]. The Hg lamp is purged in N_2 to prevent the build up of ozone from O_2 photolysis.



The light first passes through a temperature controlled Hg lamp through a band-pass filter, through a shutter assembly, and through a 2.5 cm enclosed path [Mauldin *et al.*, 1998]. Then the light illuminates the sample air flow and which initiates the photolysis in R7.

$$\frac{I_1}{I_2} = e^{-\sigma[\text{H}_2\text{O}]} \quad (1)$$

$$[\text{OH}] = (I_0 - I_1)\Omega \quad (2)$$

The concentration of OH generated can be calculated via Beer's Law shown in equations 1 and 2. In equation 1, I_0 refers to intensity of incident light, I_1 refers to intensity of transmitted light, σ refers to the absorption cross section of water vapor determined to be $7.22 \cdot 10^{-20}$ [Cantrell *et al.*, 1997], l refers to the path length. In equation 2, Ω refers to the quantum yield of OH from H_2O photolysis at 184.9 nm and is assumed to be unity [Mauldin *et al.*, 1998].

c. Part 1: Chemical Ionization of HO_2 , HO_2+RO_2

The ionization region for the chemical ionization of peroxy radicals is shown in Figure 2. The sample airflow is diluted with alternating N_2 and O_2 which are injected into the airflow at the intake of the sample tube in order to generate a 1:1 mixing ratio with the flow of sampled ambient air. N_2 is added for the HO_2 mode and O_2 is injected for the HO_2+RO_2 mode. A second front injector introduces alternating concentrations of NO and SO_2 into the airflow for a total measurement of peroxy radicals. Mass flow controllers and a series of low volume valves will control the concentrations added. The relative concentrations of O_2 and NO will determine the sensitivity to RO_2 which will allow to differentiate between HO_2 and HO_2+RO_2 modes.

In the HO_2 mode, 67.5 ppm of NO, 400 ppm of SO_2 , and 100,000 ppm of O_2 inlet concentrations allow for a measurement of the total signal in the HO_2 mode with an approximate ratio of RO_2 to HO_2 sensitivity of 1:6. The chemical reactions R19-R23 demonstrate the reaction process [Edwards *et al.*, 2003]:



For the HO₂+RO₂ mode, 15 ppm of NO, 600,000 ppm of O₂, and 1800 ppm of SO₂ inlet concentrations allow for the measurement of the total signal in the HO₂+RO₂ mode. Under these conditions, the sensitivity of RO₂ to HO₂ is approximately 1:1. In particular, if the RO₂ possesses available hydrogen atoms and can be converted into a carbonyl compound, RO₂ radicals can be measured by the SICIMS in the HO₂+RO₂ mode by first converting the RO₂ into HO₂ [Edwards *et al.*, 2003]:



It should be noted that for RO₂ species with between one and three carbon atoms, R25 is small and can be reasonable ignored. RO₂ with more than 4 carbon atoms may have an appreciable loss via reaction (R14) but the relative concentration of ambient RO₂ of these species is small in comparison with C₁-C₃ RO₂ species. Nevertheless, the total RO₂ signal can be corrected with hydrocarbon measurements and or/budgets.

After the HO₂ and HO₂+RO₂ are converted to H₂SO₄ as shown in R22, these molecules enter the chemical ionization region. Similar to the OH inlet chemical ionization region, HNO₃ enters the airflow in the sheath flow in which it is converted to NO₃⁻ ions by the ²⁴¹Am foil (R28). This ionization reaction takes about 0.22 s [Edwards *et al.*, 2003].



At the end of the reaction region, the core ions will be directed by the electrostatic lenses through an orifice, which allow only the small flow of N₂ buffer gas to pas through along with the core ions formed. The remainder of the gas is pumped from the front of the plate using a scroll pump at a rate of approximately 4 Lpm (liters per minute). Thus, the CDC region will exist at a pressure less 10⁻² torr.

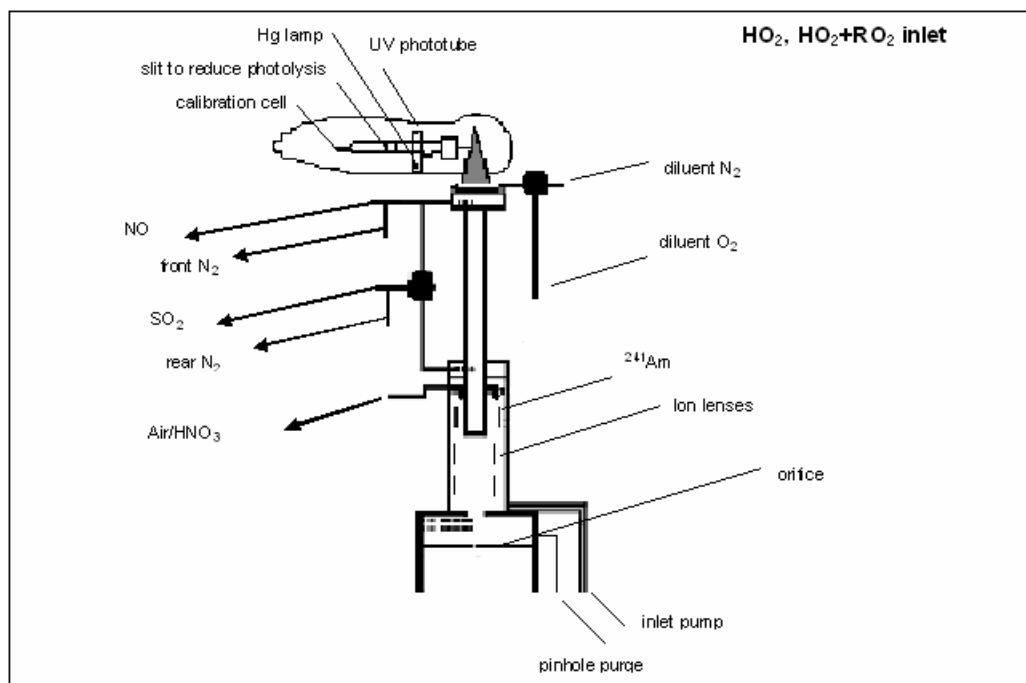


Figure 2: This depicts the HO_2 , HO_2+RO_2 inlet.

c. Part 2: Background Measurements of HO_2 , HO_2+RO_2

Because H_2SO_4 is naturally present in the troposphere, its concentrations will also lead to HSO_4^- ions in the chemical ionization region. Thus, background measurements are made and subtracted from the signal measurements to obtain a true measurement of ambient HO_2 and HO_2+RO_2 . To measure the background signal, SO_2 is added to the rear injector instead of the front injector. Thus, only NO will be added to the front injector. Thus, NO is added to the front injector. This will allow all the peroxy radicals to be converted into HONO (R23) and thus only the ambient HSO_4^- will be quantified by the mass spectrometer. Such injections will let all the peroxy radicals to be converted into HONO as shown in R23 and thus only the ambient HSO_4^- will be quantified by the mass spectrometer.

c. Part 3: Calibration of HO_2 and HO_2+RO_2

Similarly to the calibration of OH , calibration of HO_2 , HO_2+RO_2 is performed using a low pressure Hg lamp by emission of UV radiation at 184.9 nm. In order for the sample air not to be drawn from the outside but to come in from the calibration chamber, the flow of the pinhole purge will be changed to overfill the inlet at about 1-2 liters per minute. Foremost, the air is humidified. This is accomplished by passing dry hydrocarbon free synthetic air through a high-flow humidifier containing deionized water at 303 K [Edwards *et al.*, 2003]. In order to achieve desired water mixing ratios—necessary to vary HO_2 production and its measurement during calibration—the humidified air is diluted with dry air.

The airflow then enters the quartz photolysis region where the water is converted into HO₂:



The concentration of HO₂ produced is also controlled by varying the lamp distance and the slit width. In order to generate HO₂, H₂ is added while in order to generate RO₂, a hydrocarbon species is added which is usually methane (although other hydrocarbon species may also be added in order to determine what is the sensitivity of resulting RO₂ species in comparison to CH₃O₂ and HO₂ species). These radicals are converted to HO₂ via their reactions with OH. The amount of HO₂ formed from H₂O can be calculated as follows:

$$[\text{HO}_2] = (It)\sigma_{\text{H}_2\text{O}}\phi_{\text{H}_2\text{O}}[\text{H}_2\text{O}] \quad (7)$$

In this equation, $\sigma_{\text{H}_2\text{O}}$ refers to the absorption cross section of water vapor and was determined to be $7.22 \cdot 10^{-20}$ [Cantrell *et al.*, 1997]; $\phi_{\text{H}_2\text{O}}$ refers to the photolysis quantum yield of HO₂ from water vapor; (*It*) refers to the product of the lamp flux and the photolysis time which is accomplished through photolysis of a mixture of approximately 2% N₂O with the utilization of the low pressure mercury lamp. A description of the technique and particular reactions can be found in previous studies [Edwards *et al.*, 2003].

d. Part 1: Ionization of NH₃

The ionization region for the chemical ionization of NH₃ is shown in Figure 3. Measurement of NH₃ is a more direct one in that it only includes the measurement of the signal. Its measurement, however, is a more challenging one due to its polar structure causing it to adhere to most surfaces. Thus, ammonia coming off or sticking to the walls of the inlet would add error to its measurements. This difficulty is surpassed by the inlet through which the ammonia gas is let in. The air flows so quickly through the inlet—approximately 6 to 10 m/s—that the NH₃ coming off the walls would not be fast enough to make its way from the wall to the inlet into the vacuum system.

Foremost, the airflow encounters two corona needles. They are positioned so that its tip lies within the ionization region and a counter electrode positioned opposite it so that the electric potential between the two will be sufficient to create a corona discharge [Aisawa *et al.*, 1998]. A voltage of 3 – 4 kV is applied to corona needle. The ions exit the ionization region and enter into the mass spectrometer region. The corona discharge then creates a plasma which creates primary ions from the ambient air flow such as N₂⁺ and O₂⁺, created by the loss of electrons generated by the plasma [Thomas, 2001]. A grid at ground potential functions as the counter electrode. The ions are induced to accelerate due to the influence of a potential difference between the ion source and the grid held at ground potential, allowing them to pass through it. The energy of the electrons is moderated by a number of collisions with gas molecules before attaining energy where their effective ionization cross-section allows them to ionize neutral molecules. Through

collisions with gas molecules, the generated electrons generate intermediate ions, and finally formation of sample ions.

At the end of the ionization region, the airflow with the core ions will be sucked through the 0.010 inch pinhole and enter the drift tube. This form of differential pumping will reduce the pressure in the drift tube to about 2 Torr. After the drift tube, the airflow will enter the CDC.

Background measurements of NH_3 will not be necessary because there were no chemical reactions this molecule had to go through in which additional NH_4^+ ions would be introduced and amplify the signal measurement.

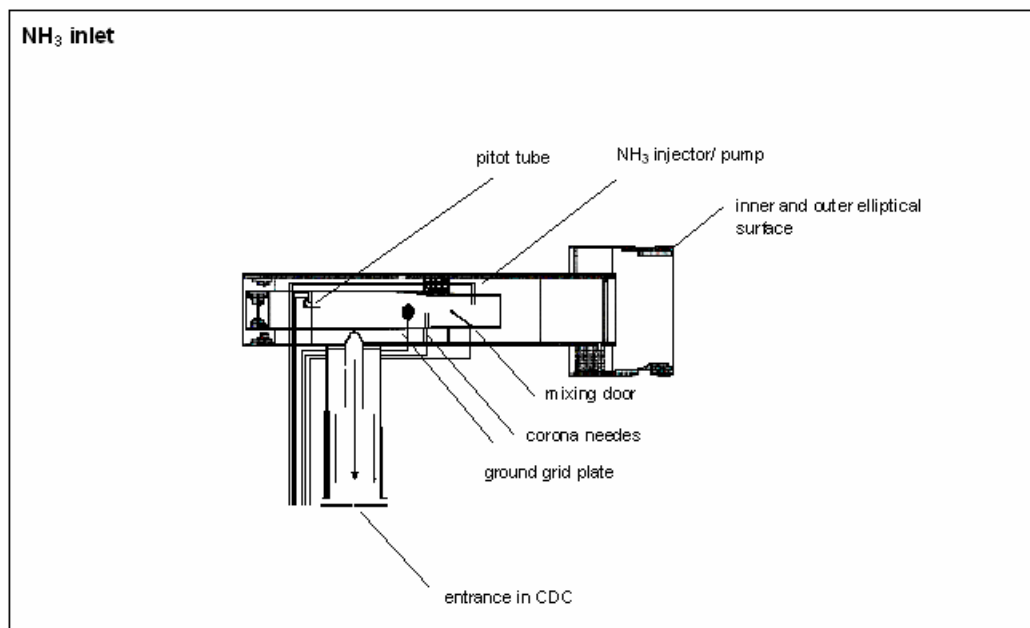


Figure 3: This depicts the NH_3 inlet.

d. Part 2: Calibration of NH_3

Calibration of ammonia is done in two parts. A known amount of ammonia is let through by turning on a pump which will pump out the outside airflow coming in and will let a certain concentration of NH_3 to enter the sample tube from a vial. By calculating the flow velocity with a pitot tube, area of the inlet, it is possible to determine the volume of gas propagating through. The door located behind the location where NH_3 is injected will be turned on to introduce turbulence into the air for mixing purposes. The ammonia molecules will then be ionized in to NH_4^+ ions as during the chemical ionization process. Also, a gas with no ammonia is let through. This step is necessary to determine how much ammonia is coming off the walls when the gas measured contains no amount of it after the ammonia coming off the walls will hit a steady state.

e. Dissociation, Transportation, Analysis, and Detection Process

The schematic for the dissociation, transportation, analysis, and detection process is shown in Figure 4. The ions and ion clusters then enter the CDC in which the fragmentation of molecules takes place through the collisions of the ions with N₂. The dissociation of the ions takes place in two subsequent steps: First, the fraction of the ions' kinetic energy is transferred into internal. Second, the transfer of energy results in bond breakage and dissociation of the ion clusters into individual ions [Shukla, Futrell, 2000]. After leaving the CDC, the ions are directed by electrostatic lenses into the differentially pumped chamber which consists of three turbo pumps. Each pumps out air at approximately 1000 sccm and creates a vacuum with an approximate pressure of 10⁻⁵ torr. Such a vacuum is necessary in order to create a mean free path in which the ions would reach the mass analyzer before reacting.

After the ions exit the vacuum region, they will pass through a skimmer and enter the conical octopole and finally, the detection region. In previous studies, the ions were guided from CDC into the quadrupole mass spectrometer using ion optics. The necessity for a strong focusing mechanism is because when the ions are generated in the plasma emerge from the skimmer cone, they undergo a rapid expansion as the pressure is reduced from 760 to 10⁻⁵ Torr [Thomas, 2001]. The ion optics also function to stop particulates, neutral species, and photons into getting into the mass analyzer region by decreasing the background noise [Thomas, 2001]. The ion optics consisted of three ion lens in series with each other which electrostatically directed ions by placing voltage on the lens (50- 120 eV). Each ion lens functions as an oppositely charged ring which focuses ions to a beam of a particular size. The conical octopole, which replaces ion optics in this study, is able to focus the ions to a beam of a smaller size and thus increase signal 10 to 100 fold. The octopole is constructed of eight elongated electrodes which are placed symmetrically about the axis. It is tilted from one tapered pole to the other by approximately 5° [Rottgen *et al.*, 2006]. The construction of the octopoles is such that neighboring poles have opposite voltage which confines the ion beam to this potential.

The ions then enter the quadrupole mass spectrometer and detector. Basically, the quadrupole mass analyzer sorts the ions while the detector gives off a signal when it is struck. The four metal rods will guide the ions into the detection region, with two opposite rods having radio frequency (rf) and two others having direct current (dc). By tuning the two currents, it is possible to select specific ions for detection. This construction will affect the path of the ions so that for a specific rf and dc, only ions of a certain mass to charge ration will pass through while all the others will be filtered. Following the mass analysis process, the ions will reach the detector—channeltron electron multiplier to which a voltage of about 3 kV is typically applied.

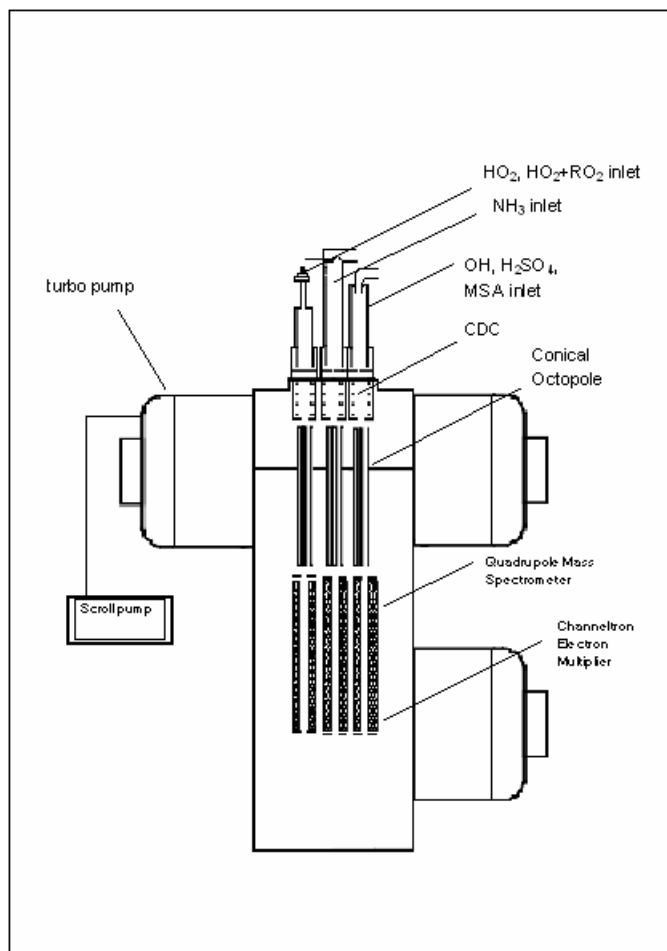


Figure 4: This depicts the Selective Ion Chemical Ionization Mass Spectrometer

f. Part 1: OH Measurement

By measuring the amount of ions formed ($H^{34}SO_4^-$) it is possible to determine the amount of OH actually formed. The direct calculation of OH, H_2SO_4 , and MSA is shown in equations 4-6 in which C is the calibration coefficient. It depends on the rate coefficient of the reaction, the reaction time in the ion reaction region, and the difference in efficiency with which the ions are detected [Mauldin *et al.*, 1998].

$$[OH] = C \cdot \frac{H^{34}SO_4^-}{NO_3^-} \quad (4)$$

$$[H_2SO_4] = C \cdot \frac{HSO_4^-}{NO_3^-} \quad (5)$$

$$[MSA] = C \cdot \frac{(CH_3)SO_3^-}{NO_3^-} \quad (6)$$

In order to get the real value of OH, the value of $H^{34}SO_4^-$ (signal) is subtracted from the value of $H^{34}SO_4^-$ (background) at mass 99 [Mauldin *et al.*, 1998]. This calculation usually takes 30 s and consists of several separate measurements. The first 8 s measurement incorporates the

signal measurement during which $^{34}\text{SO}_2$, HNO_3 , and N_2 are added. Then, propane is added to measure the background. Because it takes a couple of seconds for all of the $\text{H}^{34}\text{SO}_4^-$ to be titrated out, other measurements are taken at this time which consist of a 0.5 s measurement of NO_3^- at mass 62, 2.5 s measurement of MS^- at mass 95, and a 4 s measurement of HSO_4^- at mass 97. At the end of the 8 s, the propane is turned off. Because it takes a couple of seconds for the reaction to reach equilibrium, a set of three measurements is taken again which include a 0.5 s measurement of NO_3^- at mass 62, 2.5 s electronic background measurement at mass 10, and 4 s HSO_4^- measurement at mass 97.

f. Part 2: HO_2 , HO_2+RO_2 Measurement

The calculation technique for measurements of HO_2 , HO_2+RO_2 is more complicated than the one for OH as the conversion of these radicals to detect ions includes a variety of competing reactions. The calculation includes the determination of concentration of H_2SO_4 from the HSO_4^- ions detected and can be accomplished via equation 5. The latter calculations can be accomplished via equations 7 and 8 (discussed in more detail in [Edwards et al., 2003]).

$$\frac{[\text{H}_2\text{SO}_4]}{[\text{HO}_2]} = \left(\frac{k_9[\text{SO}_2]}{k_{12}[\text{NO}]} \right) \left(1 + \frac{C e^{-Dt} - D e^{-Ct}}{G^{1/2}} \right) \quad (7)$$

$$\frac{[\text{H}_2\text{SO}_4]}{[\text{RO}_2]} = \alpha_{\text{RO}_2} \left(\frac{k_9[\text{SO}_2]}{k_{12}[\text{NO}]} \right) \left(1 + \frac{C e^{-Dt} - D e^{-Ct}}{G^{1/2}} \right) \quad (8)$$

In these equations, C, D, and G are variables which depend upon the concentrations of NO and SO_2 and the rate coefficients k_8, k_9, k_{12} for R19, R20, and R23; α_{RO_2} is a variable that refers to relative conversion efficiency of RO_2 radicals to HO_2 and depends upon the rate coefficients $k_{13}, k_{14}, k_{15}, k_{16}, k_{\text{decomp}}$, and $k_{(\text{RO}_2+\text{SO}_2)}$ for R24, R25, R26, R27, decomposition and isometrization processes, RO reaction with SO_2 leading to HO_2 .

The HO_2 , HO_2+RO_2 measurement consists of four basic parts. Foremost, NO_3^- is measured at mass 62 for approximately 10 seconds and HSO_4^- is measured for 8 seconds in the HO_2+RO_2 signal mode. Then, mass 20 is measured for 4 seconds and HSO_4^- is measured for 8 seconds in the HO_2+RO_2 background mode. Thus, this gives the measurement of sulfuric acid every 7 seconds and a measurement of HO_2+RO_2 radical every 30 seconds. Under HO_2 mode, NO_3^- is measured at mass 62 for approximately 10 seconds and NO_3^- is measured at mass 97 for approximately 8 seconds in the HO_2 signal mode. Last, mass 70 for 4 seconds and NO_3^- is measured at mass 97 for 8 seconds in the HO_2 mode. This gives the measurement of sulfuric acid every 7 seconds and a measurement of HO_2 every 30 seconds. The measurement of mass 20 and 70 is a measurement of electronic noise and is necessary in order to make sure that the electronic noise is not too high under the channeltron conditions set.

f. Part 3: NH_3 Measurement

An integrated measurement of ammonia is made every 15s. It should be noted that the detector records measurements of other gases ionized as well which include acetone, methanol, and

aldehyde. The instrument is not calibrated for these measurements, however, and thus the data is not further analyzed.